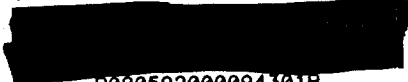


CEBAF-PR-87-010 VWC3
David Douglas
Perturbation Effect\ort System
* 020592000094301



020592000094301

Master Copy

CEBAF



0205 9100 002 794 6

CEBAF-PR-87-010

PERTURBATION EFFECTS IN THE CEBAF BEAM
TRANSPORT SYSTEM

*D. R. Douglas and R. C. York
Continuous Electron Beam Accelerator Facility
12070 Jefferson Avenue
Newport News, VA 23606*

PERTURBATION EFFECTS IN THE CEBAF BEAM TRANSPORT SYSTEM*

D. R. Douglas and R. C. York
CEBAF, 12070 Jefferson Avenue, Newport News, VA 23606

Introduction

The CEBAF accelerator design is a recirculating, superconducting, cw, electron linac producing beams with energies of 0.5 to 4.0 GeV. The lattice design of this machine is described elsewhere¹. Here, we will discuss the machine chromatic correction scheme and the anticipated machine performance in the presence of synchrotron radiation excitation, optical perturbations such as misalignments, miscalibrations, and magnet inhomogeneities, and errors in the extraction process.

Chromatic Aberrations and Corrections

The linear lattice of CEBAF recirculation transport lines has a significant dependence of the betatron phase advance on momentum. Typically, $\partial Q_{x,y}/\partial(\Delta p/p) \sim -10$ to -15 in each line. Correction of chromatic aberrations is, therefore, provided using eight sextupoles in each recirculation beam line to maintain the inter-linac betatron match and the overall phase advance.

Two types of correction have been investigated. The first is a local compensation of the arc beam line chromatic effects using two sextupole families. In this scheme, the arc beam lines are second order achromats². Spreader and recombiner aberrations are uncorrected. The resulting linac-to-linac transport line therefore has a significant residual phase advance variation ($\partial Q/\partial(\Delta p/p) \sim -5$). The second solution is based on a scheme due to Collins³, and employs two sextupole families to compensate the variation in phase advance with momentum across a complete recirculation path for the particular betatron functions transported through that path. Correction of the linear variation of the phase advance with momentum is exact. The residual aberrations are acceptable with betatron parameter variations of a few percent and phase advance variations of $\approx 10^{-3}$ over 10 full beam momentum widths. As the arc beam line lattice comprises four quarter-wavelength periods¹, geometric aberrations are suppressed. Moreover, the method is extensible though the use of four sextupole families to correct the betatron phase advance and either β or α (but not both).

Magnetic Error Effects

A dipole error ΔB over length l deflects the beam through an angle $\Delta B/B\rho$. This translates to a downstream displacement $d_{x \text{ or } y}$ given by:

$$d = \sqrt{\beta_e \beta_o} \left(\frac{\Delta B l}{B\rho} \right) \sin 2\pi(Q_o - Q_e) \quad (1)$$

(subscripts e and o refer, respectively, to the error and observation points). If there are N random error sources in a given beam line, and if linearity is assumed, Eqn. (1) may be summed over all sources and averaged over an ensemble of machines to obtain an rms displacement at the observation point due to all errors:

$$\langle d \rangle = \sqrt{\frac{N}{2} \beta_o \bar{\beta}} \left(\frac{\Delta B l}{B\rho} \right) \quad (2)$$

where $\bar{\beta}$ is the mean beta function at the error sites and $\langle \rangle$

denotes the rms of the enclosed quantity. This result is applied below to estimate the effect of quadrupole misalignments and dipole powering errors.

Misalignment Effects

Analytic Estimates The angular displacement generated by a quadrupole misaligned by δr is $\Delta B/B\rho = kl\delta r$ (with $r = x$ or y and $k = B'/B\rho$). Use of Eqn. (2) gives the rms orbit displacement at the end of a transport line generated by rms misalignments $\sigma_{x,y}$ of N quadrupoles of rms strength $\langle k \rangle$.

$$\langle d_{x,y} \rangle = \sqrt{\frac{N}{2} \beta_{x,y}^{\text{end}} \bar{\beta}_{x,y}} \langle k \rangle l \sigma_{x,y} \quad (3)$$

For the CEBAF recirculator transport lines, $\langle k \rangle \sim 1.25 \text{ m}^{-2}$, $l = 0.3 \text{ m}$ and $\bar{\beta}_{x,y} \sim 50 \text{ m}$. Results for each beam line are given in Table 1, assuming an rms quadrupole misalignment of 0.2 mm in both planes. In this and following tables, E1, E2, E3 and E4 refer to the four recirculation lines following the first linac and W1, W2 and W3 refer to the three lines following the second linac. We remark that if the spreaders/recombiners are eliminated, the sensitivity parameter $S_{x,y} = (N \beta_{x,y}^{\text{end}} \bar{\beta}_{x,y}/2)^{1/2} \langle k \rangle l$ is approximately 20 for horizontal and 7 for vertical motion. The spreader/recombiners thus comprise a source of substantial sensitivity.

For the CEBAF linac segments, $\langle k \rangle \sim 1.24, 0.24, 0.15, \text{ and } 0.10 \text{ m}^{-2}$ for the first, second, third, and fourth passes of the first linac segment, and similarly $\langle k \rangle \sim 1.24, 0.53, 0.34, \text{ and } 0.26 \text{ m}^{-2}$ for the second linac segment, and $l = 0.15 \text{ m}$. Table 2 gives the betatron parameters and rms final orbit excursions on each pass.

Numerical Modeling Misalignment effects and their correction were studied using DIMAD⁴. Both linac and recirculation arc elements were misaligned assuming a Gaussian distribution (truncated at 6σ), and the orbit corrected. In the recirculation beam lines, quadrupoles, sextupoles and beam position monitors were randomly misaligned with positional errors with $\sigma_{x,y} = 0.2 \text{ mm}$ and pitch/yaw errors with $\sigma_{x',y'} = 2.0 \text{ mrad}$. Orbit analysis and correction was then done. Beam x and y positions were assumed read by beam position monitors adjacent to all quadrupoles, and dipole orbit correctors were varied to minimize all monitor readings using a least squares fit. Correction in each plane was provided by dipoles adjacent to quadrupoles focusing in that plane. The resulting uncorrected and corrected rms and peak orbit excursions are summarized in Table 3. Preliminary studies indicate there is no unexpected dependence on random seed.

The linac segments were modeled with quadrupole misalignments with $\sigma_{x,y} = 0.2 \text{ mm}$ and $\sigma_{x',y'} = 1.33 \text{ mrad}$. In addition, steering due to cavity pitch/yaw errors with $\sigma_{x',y'} = 0.8 \text{ mrad}$ was simulated. The correction process is, in this case, complicated by the fact that four beams simultaneously pass through the linac segments. However, the deflections generated by quadrupole and cavity misalignments scale inversely with particle momentum, as do the compensating deflections from correction dipoles. Thus, a careful correction of the first pass orbit will provide corrections for all subsequent passes. Results confirm this; rms and peak orbit excursions for the

*Supported by D.O.E. contract #DE-AC05-84ER4015

uncorrected and corrected machine are given in Table 4. First pass correction was accomplished using a scheme identical to that described for the recirculation arcs with the exception that correction dipoles for both planes were assumed at each quadrupole. Preliminary studies indicate there is no unexpected dependence on random seed.

Effect of Magnet Mispowering

Errors in Dipole Powering Analytic estimates based on Eqn. (2) and numerical simulations using DIMAD indicate random arc dipole powering errors with rms values of 0.01% will produce design orbit errors of 1.5 mm at the end of the lowest-energy beam line (the most sensitive, because it has only 16 dipoles). Systematic dipoles errors cancel completely over the beam line length because the beam line is an achromat. For this reason, the dipoles in a given beam line will be on a common circuit; any powering errors will then be systematic. Nonetheless, the dipole powering will be held to $\Delta B/B = 10^{-5}$ so that the energy of the beam may be precisely measured.

Numerical simulation indicates that dipole powering errors even at the 0.01% level generate no significant path length error and will therefore have no influence on the rf phase match between linac segments.

Quadrupole Powering Errors Analytic estimates and numerical simulations both indicate that for arc beam lines alone, quadrupole powering errors of 0.1% produce rms betatron function mismatches of 0.4% in β and 0.004 in α , as well as rms tune variations on the order of 0.002. These are acceptably small; arc beam line quadrupoles will be powered to a 0.1% tolerance. If spreader/recombiners are included, the rms mismatches increase to the order of 10% in β , 0.1 in α , and 0.01 in tune. Though not excessive, these are large enough for concern; a 0.01% tolerance in spreader/recombiner quadrupoles is therefore contemplated. Simulations with DIMAD indicate that quadrupole errors in the presence of misalignment have no significant effects on the position and correction of the misaligned central orbit.

The linac quadrupole powering will be stable to the 0.1% level; numerical simulations indicate that no observable beam degradation occurs at this tolerance.

Magnetic Inhomogeneities

In a single-pass machine, the primary effect of magnetic inhomogeneities is confined to low-order betatron mismatches. We have therefore investigated the impact on the optics of sextupole errors in the recirculation arc dipoles. Numerical simulation indicates that the primary effect of a systematic sextupole producing $\Delta B/B$ of 10^{-4} at 1 cm is to generate an effective chromaticity on the order of 10% of the ideal value of the chromaticity of the entire recirculation path. This is readily compensated with the standard chromaticity sextupoles. Numerical studies using DIMAD indicate that a random sextupole component of the same magnitude has little additional impact on the second-order optics. In a study using 5 random seeds and the above systematic sextupole, the rms chromaticity error generated when a random sextupole with $(\Delta B/B)_{rms} = 10^{-4}$ at 1 cm was activated was within $\approx 20\%$ of the chromaticity error obtained from the systematic term alone. Finally, simulation indicates that systematic and random errors at these levels generate no significant geometric or chromatic aberrations.

Effects of Radiative Excitation

Analytic Estimates of synchrotron radiation induced emittance and momentum spread growth are displayed in Figure 1. The results, based on relations given in a companion paper¹, illustrate the cumulative increases for all recirculations, and include the effect of adiabatic damping. The results are well below the design values of the machine, with $\Delta\epsilon = 3.4 \times 10^{-11}$ m-rad compared to a damped emittance value of $\epsilon = 5 \times 10^{-10}$ m-rad at 4 GeV and $(\sigma_E/E)_{induced} = 1.2 \times 10^{-5}$ compared to the design value of $(\sigma_E/E) = 2.5 \times 10^{-5}$ at 4 GeV.

Numerical Simulations have been used to verify analytical estimates. Two independent numerical simulations have been performed. The first used the synchrotron radiation simulation feature of DIMAD to model the motion of 10,000 particles through the beam lines. This simulation assumed an approximate, Gaussian distribution for the radiated photon energy and number spectra, and thus was most appropriate to modeling motion in the high-energy beam lines. The second, described elsewhere⁵, employed statistics that were correct in the details of the distributions describing the radiation, and hence was appropriate for modeling motion in all beam lines. Results from both simulations were consistent and in agreement with analytic estimates.

Errors in Extraction Processes

Extraction from the accelerator is accomplished using 2.5 GHz rf separators. Due to the finite microbunch length ($\pm 0.5^\circ$) the head and tail of an individual microbunch receive significantly different transverse deflections from the rf separator. This leads to a dilution of the beam transverse phase space. Therefore, the extraction region optics have been designed so as to minimize the rf separator kick required for extraction¹, thereby minimizing the emittance dilution from this source. Analytic estimates of the magnitude of the emittance dilution are summarized in Table 5; numerical studies verify the presence and magnitude of the effect.

Additionally, phase and amplitude errors in the rf separator will lead to variations in bunch centroid position downstream of the separator. This also corresponds to an emittance dilution. The magnitude of this effect increases with increasing separator deflection; the extraction channel optics, which were designed to minimize the required separator kick (and thus, the effect of errors in the deflection) therefore reduce the effect of such errors. For example, in the full-energy extraction line (4.0 GeV, where the beam is most sensitive to such errors by virtue of its small emittance), a separator phase error of 1° and an amplitude error of 1% lead to a factor of three emittance dilution⁶.

Table 1: Arc Misalignment Sensitivity

$$S = \sqrt{N\beta^{end}\bar{\beta}/2} \langle k \rangle l$$

$$\langle \langle d_x \rangle, \langle \langle d_y \rangle \rangle \text{ for } \sigma_{x,y} = 0.2 \text{ mm}$$

beam line	β_x^{end} (β_y^{end}) [m]	S_x (S_y)	$\langle \langle d_x \rangle \rangle$ ($\langle \langle d_y \rangle \rangle$) [mm]
E1	2.6 (40.6)	22.8 (90.2)	4.56 (18.0)
W1	90 (90)	134 (134)	26.8 (26.8)
E2	28.9 (46.4)	76.1 (96)	15.2 (19.2)
W2	90 (90)	134 (134)	26.8 (26.8)
E3	17.7 (27.7)	60.0 (74.5)	12.0 (14.9)
W3	90 (90)	134 (134)	26.8 (26.8)
E4	97.3 (122.9)	132 (148)	26.4 (29.6)

Table 2: Linac Misalignment Sensitivity

$$S = \sqrt{N\beta_{\text{end}}\bar{\beta}/2} \langle k \rangle l$$

$((d_x), (d_y))$ for $\sigma_{x,y} = 0.2$ mm

linac/pass	β_x^{end} [m]	(β_y^{end}) [m]	$\bar{\beta}_x$ ($\bar{\beta}_y$) [m]	S_x (S_y)	$\langle d_x \rangle$ ($\langle d_y \rangle$) [mm]
1/1	3.00 (44.7)	20 (20)	5.1 (19.6)	1.0 (3.9)	
1/2	33.3 (59.9)	70 (70)	6.2 (8.4)	1.2 (1.7)	
1/3	22.2 (33.0)	105 (105)	3.7 (4.6)	0.74 (0.92)	
1/4	77.1 (98.6)	140 (140)	5.7 (6.5)	1.1 (1.3)	
2/1	39.3 (2.67)	20 (20)	18.4 (4.8)	3.7 (0.96)	
2/2	32.3 (11.6)	55 (55)	11.9 (7.1)	2.4 (1.4)	
2/3	21.1 (11.6)	70 (70)	7.0 (5.2)	1.4 (1.0)	
2/4	65.2 (42.4)	75 (75)	9.5 (7.6)	1.9 (1.5)	

Table 3: Arc Misalignment and Correction (in mm)

beam line	uncorrected		corrected	
	x (y) rms	x (y) peak	x (y) rms	x (y) peak
E1	6.9 (21)	21 (-55)	0.20 (0.19)	0.93 (0.44)
W1	16 (12)	-59 (40)	0.18 (0.14)	-0.61 (0.45)
E2	9.5 (12)	56 (28)	0.17 (0.17)	-0.52 (-0.47)
W2	16 (5.8)	88 (21)	0.18 (0.18)	-0.41 (-0.45)
E3	6.7 (11)	-22 (-33)	0.22 (0.17)	-1.04 (0.39)
W3	7.8 (22)	-22 (-55)	0.16 (0.22)	-0.50 (0.78)
E4	6.4 (14)	-16 (38)	0.22 (0.15)	-0.92 (-0.40)

Table 4: Linac Misalignment and Correction (in mm)

linac/pass	uncorrected		corrected	
	x (y) rms	x (y) peak	x (y) rms	x (y) peak
1/1	1.1 (1.2)	8.2 (3.6)	0.17 (0.20)	0.49 (0.71)
1/2	0.86 (0.49)	2.5 (1.0)	0.91 (0.57)	0.80 (1.4)
1/3	0.65 (0.51)	1.4 (1.2)	1.1 (0.57)	2.5 (1.2)
1/4	0.54 (0.42)	1.1 (1.1)	0.96 (0.48)	2.3 (0.98)
2/1	1.6 (0.50)	5.4 (4.5)	0.17 (0.20)	0.44 (0.76)
2/2	0.90 (0.50)	2.1 (1.3)	0.50 (0.32)	1.4 (0.85)
2/3	1.3 (0.58)	3.2 (1.2)	0.85 (0.53)	1.9 (1.2)
2/4	1.4 (0.64)	2.7 (1.3)	1.1 (0.61)	2.4 (1.4)

Table 5: RF Separator Induced Emittance Dilution Factors
($\epsilon_{\text{effective}}/\epsilon_{\text{ideal}}$ shown for three beams at correlated energies)

Energy of Beams (GeV)			
1	2	3	4
1.0	1.34		1.92
1.0		1.35	2.06
1.0			1.34, 2.96
	1.0	1.50	2.26
			1.50, 3.20
		1.0	1.62, 3.38
			2.72, 1.76, 1.76

References

1. R. C. York and D. R. Douglas, these proceedings.
2. K. L. Brown, I.E.E.E. Trans. Nuc. Sci. **NS-26**, 3,(1979).
3. D. Douglas, A. Garren and F. Dell, LBL-17984 (June, 1984).
4. R. V. Servranckx *et al.*, SLAC Report 285 UC-28 (A) (May, 1985).
5. B. Norum, CEBAF-TN0019 (5 Nov. 1985).
6. CEBAF Design Handbook, Chap. 4.5 (19 Dec. 1986).

*Supported by D.O.E. contract #DE-ACO-84ER4015

Figure 1. Cumulative emittance degradation and momentum spread generated by synchrotron radiation excitation; values plotted at start and end of each transport line. Line # 1 is E1, line # 2 is W1, line # 3 is E2, and so forth.

Figure 1a). Emittance blow-up from synchrotron radiation.

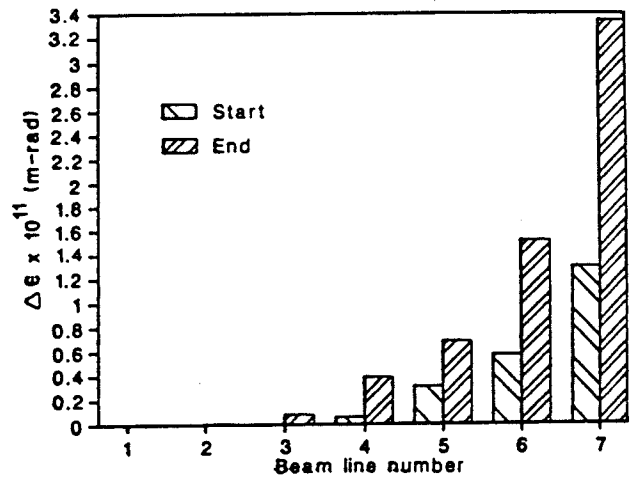


Figure 1b). Momentum spread generated by synchrotron radiation

